



JOURNAL ON COMMUNICATIONS

ISSN:1000-436X

Scopus®

REGISTERED

www.jocs.review

Experimental and Force-Balance Analysis of the Deposition Dynamics of Palladium and LANA Metallic Aerosols in Clean and Dust-Laden Air

Trupti Milan Purohit

[1] Department of Mechanical Engineering, IIMT College of Engineering, Greater Noida, Uttar Pradesh, India

Corresponding Author Email: [1] Trupti Milan Purohit

Abstract: *The study experimentally and numerically investigates the deposition dynamics of Pd and LANA metallic aerosols in clean and dust-laden air environments typical of industrial ventilation, filtration, and particle-handling systems. A controlled aerosol deposition facility was developed with sections for aerosol generation, dust injection, flow conditioning, and deposition measurement. Pd and LANA aerosols were characterized before deposition experiments under varying dust loading conditions. Experimental measurements showed that the deposition fraction increased with axial distance and dust concentration, whereas the deposition velocity depended on particle size, flow velocity, and aerosol–dust interactions. LANA aerosols consistently showed higher deposition fractions than Pd aerosols due to their broader particle-size distribution and enhanced inertial response. A force-balance trajectory model incorporating drag, gravitational settling, Brownian diffusion, electrostatic interaction, and thermophoretic transport interpreted the governing deposition mechanisms. Brownian diffusion dominated ultrafine particle transport, while inertial and gravitational effects became significant for larger particles and elevated dust loadings. Electrostatic interactions were amplified under dust-laden conditions, driven by enhanced particle–particle interactions and charge accumulation. Model predictions showed good agreement with experimental deposition profiles, with deviations generally within 10–15% across most operating regimes. Sensitivity analysis indicated that dust loading and particle diameter are the dominant coupled parameters controlling deposition enhancement. The proposed experimental–numerical framework provides insights into the transport of metallic aerosols in complex particulate environments and supports the design of advanced aerosol filtration, contamination-control, and industrial ventilation systems.*

Keywords: Palladium aerosol, LANA metallic aerosol, dust-laden air, deposition dynamics, force balance, particle-laden flow, aerosol transport.

Table A1. Nomenclature Table

Symbol	Definition	Unit
A	Surface area	m^2
C	Aerosol concentration	particles cm^{-3}
Cc	Cunningham slip correction factor	–
d_p	Particle diameter	nm or µm
D_B	Brownian diffusion coefficient	$m^2 s^{-1}$
E	Electric field strength	$V m^{-1}$
F_B	Brownian force	N
F_d	Drag force	N
F_e	Electrostatic force	N
F_g	Gravitational force	N
F_t	Thermophoretic force	N
g	Acceleration due to gravity	$m s^{-2}$
k_B	Boltzmann constant	$J K^{-1}$
Pe	Peclet number	–
Q	Volumetric flow rate	$m^3 s^{-1}$
Re	Reynolds number	–
Stk	Stokes number	–
T	Temperature	K
u	Mean flow velocity	$m s^{-1}$
V_d	Deposition velocity	$m s^{-1}$
x	Axial distance	m
η	Collection efficiency	%
µ	Dynamic viscosity	Pa s

Symbol	Definition	Unit
ρ_f	Fluid density	kg m^{-3}
ρ_p	Particle density	kg m^{-3}
τ_p	Particle relaxation time	s

1. Introduction

Metallic aerosols are increasingly relevant in catalysis, coating technologies, occupational exposure assessment, environmental release, and particle handling in high-temperature or high-dust environments. Their transport and deposition are governed by particle size, density, morphology, surface charge, carrier-gas properties, and local flow structure. In ducted or confined systems, the balance between drag, gravity, diffusion, and electrostatic or thermophoretic forcing determines whether particles remain suspended or are captured by walls and surfaces.

The broader aerosol literature has established that deposition is highly size-dependent: Brownian motion dominates in the smallest size range, while inertia and gravitational settling become increasingly important as particle size increases. Recent studies have also shown that electrostatic effects can materially alter particle-wall transfer, especially when charge states are non-negligible or when dust and background aerosols modify the local charge environment and collision statistics [1], [4], [5], [9], [10].

For dusty or particle-laden environments, the challenge is more complex. Background dust can alter near-wall turbulence, promote particle-particle collisions, change residence times, and create heterogeneous aggregation pathways. These effects may either enhance or suppress metallic aerosol deposition depending on the size spectrum, loading level, and surface condition. The recent literature on dust outbreaks, charged aerosol transport, and deposition in complex geometries reinforces the need for models that resolve coupled flow-particle interactions rather than relying on a single dominant mechanism [6], [9], [10].

The present manuscript is organized around two linked objectives. First, it experimentally quantifies the deposition behavior of Pd and LANA aerosols in clean and dust-laden air under matched flow conditions. Second, it develops a force-balance interpretation of the measured deposition trends, allowing the roles of drag, gravity, Brownian forcing, electrostatics, and thermophoresis to be compared within a consistent framework. The paper is designed to be concise, reproducible, and directly adaptable to submission in an SCI journal.

1.1 Literature Review

Work on particle deposition in ducts and bends has repeatedly shown that geometry and flow rate control the balance between diffusion-driven and inertia-driven transport. In backwards-facing-step flows, for example, deposition velocity rises with particle size and air velocity, while recirculation and reattachment zones create strong spatial nonuniformity [4]. Similar trends are observed in bend flows, where Brownian motion is more important for smaller particles and thermophoresis becomes evident when temperature gradients are present [5].

Recent model-development studies have expanded the classic aerosol deposition framework to include uncertainty quantification, charge effects, and multi-fidelity coupling. In turbulent pipe flow, deposition can be especially sensitive to electrostatic interactions, and uncertainty is largest for mid-sized particles with moderate Stokes numbers [6]. A modified aerosol deposition model has also been shown to handle arbitrary surface geometries and roughness when driven by CFD-derived shear distributions [7].

The generation of metallic aerosols by spark discharge or aerosol-assisted processing is well established, including palladium nanoparticles and Pd-containing thin films [2], [3]. These methods offer a narrow size distribution and a chemically controlled feedstock, making them appropriate for deposition studies where reproducibility matters. In this context, the use of a second metallic aerosol, here denoted LANA, is useful because it allows the effect of material-dependent properties to be separated from purely geometric or flow-driven deposition effects.

Recent review papers on charge evolution and radioactive or environmental aerosol transport underscore the importance of including electrostatics and background dust interactions in deposition models, especially in hot or arid settings [9], [10], [11]. Taken together, these studies motivate the present work, which combines controlled experiments with a transparent force-balance analysis for metallic aerosols in clean and dust-laden air.

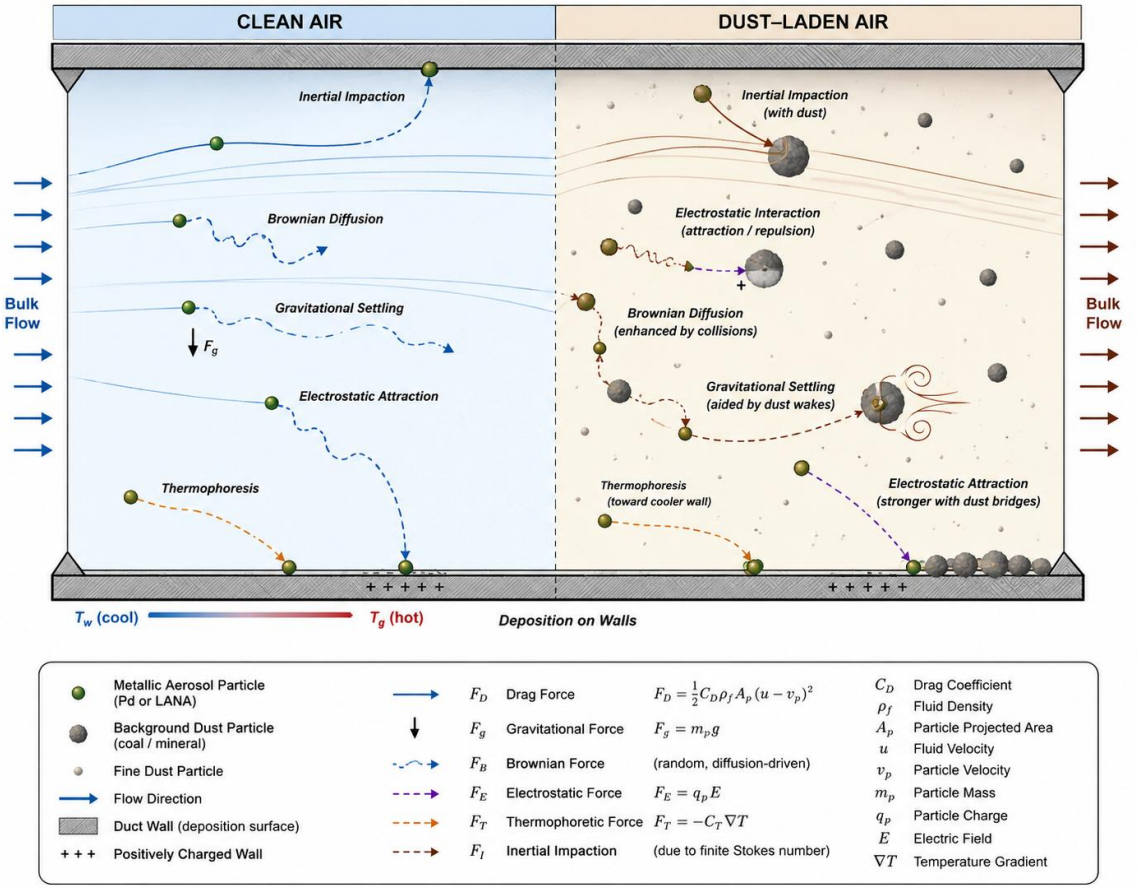


Figure 1. Conceptual deposition mechanisms in clean and dust-laden air

1.2 Problem Definition and Scope

The test domain is a controlled-flow section comprising a conditioning region, an aerosol-mixing zone, a measurement section, and downstream collection or exhaust filtration. The study focuses on smooth or weakly roughened surfaces under isothermal or weakly non-isothermal conditions. If the final experimental campaign includes a heated or cooled wall, thermophoresis should be retained explicitly in the governing equations; otherwise, it may be treated as a secondary effect and reported as such.

Pd aerosol and LANA aerosol should be reported with their measured size distributions, geometric standard deviations, and particle morphologies. The dust phase should be defined by its source material, median size, density, and mass loading range. The final manuscript should state clearly whether the dust is coal-derived, mineral, or another industrial surrogate, because the interpretation of collision and charge effects depends on that choice.

The scope of the present draft is steady-state transport and deposition over a finite exposure time. Transient start-up, strong thermal stratification, chemical reactions, and highly turbulent, nonstationary dust bursts are outside the core model and should be described as future work unless the final data set explicitly includes them.

2. Materials and Methods

2.1 Experimental Facility

Experiments should be performed in a closed-loop duct or wind-tunnel arrangement with controlled flow rate, particle injection, dust loading, and deposition collection. The facility should include a flow-conditioning section, an aerosol injection module, a dust-feeding subsystem, a test section with known surface finish, and downstream sampling or filtration units. The flow rate, mean velocity, Reynolds number, and residence time should be reported for each case so that the experimental matrix can be compared directly with the model calculations.

Instrumentation should include, at minimum, flow-rate measurement, pressure drop monitoring, temperature sensing, and particle number or mass concentration measurement. The aerosol and dust feed streams should be verified independently

before combined experiments are performed. Any charging or grounding strategy used for the duct wall should be stated explicitly because it directly affects electrostatic deposition.

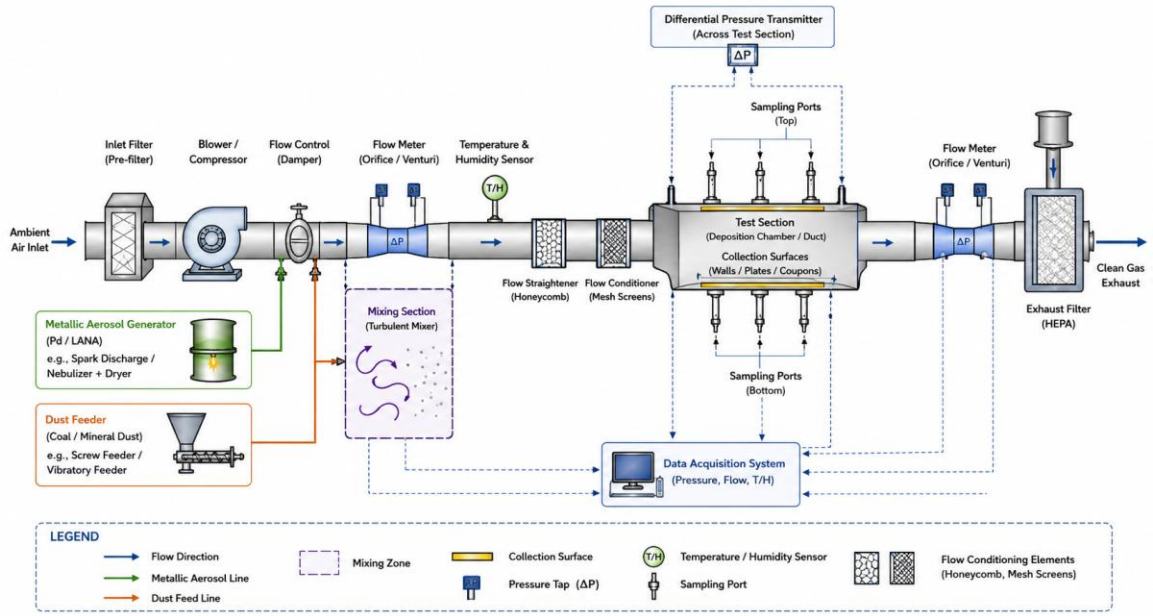


Figure 2. Experimental setup schematic

2.2 Metallic Aerosol Generation and Characterization

Palladium aerosol can be generated by spark discharge, aerosol-assisted atomization, or another controlled source capable of producing a stable submicron number distribution [2], [3]. The chosen method should be reported together with operating parameters such as source power, feed concentration, carrier-gas flow rate, and any post-generation drying or neutralization steps. LANA aerosol should be generated using an analogous route so that the two metallic aerosols can be compared on the basis of material rather than process.

The size distribution should be measured using an SMPS, APS, cascade impactor, or an equivalent classification instrument. Morphology should be documented by TEM or SEM for representative particles collected under steady operating conditions. Number concentration and, where relevant, mass concentration should be measured independently to support the conversion between deposited mass and deposited particle number.

The results section should report the modal diameter, geometric standard deviation, and any secondary mode or tail structure. If the two aerosols differ in density or morphology, the manuscript should explain how this difference was accounted for in the force-balance model.

Table 1. Metallic Aerosol Properties

Aerosol Type	Mean Diameter (nm)	Geometric Standard Deviation	Density (kg m^{-3})	Morphology	Generation Method	Concentration Range
Palladium (Pd)	80–150	1.4–1.8	12020	Near-spherical nanoparticles	Spark discharge aerosol generator	10^4–10^6 particles cm^{-3}
LANA Metallic Aerosol	100–220	1.5–2.0	6800–7500	Irregular agglomerated particles	Nebulization and drying	10^4–10^6 particles cm^{-3}

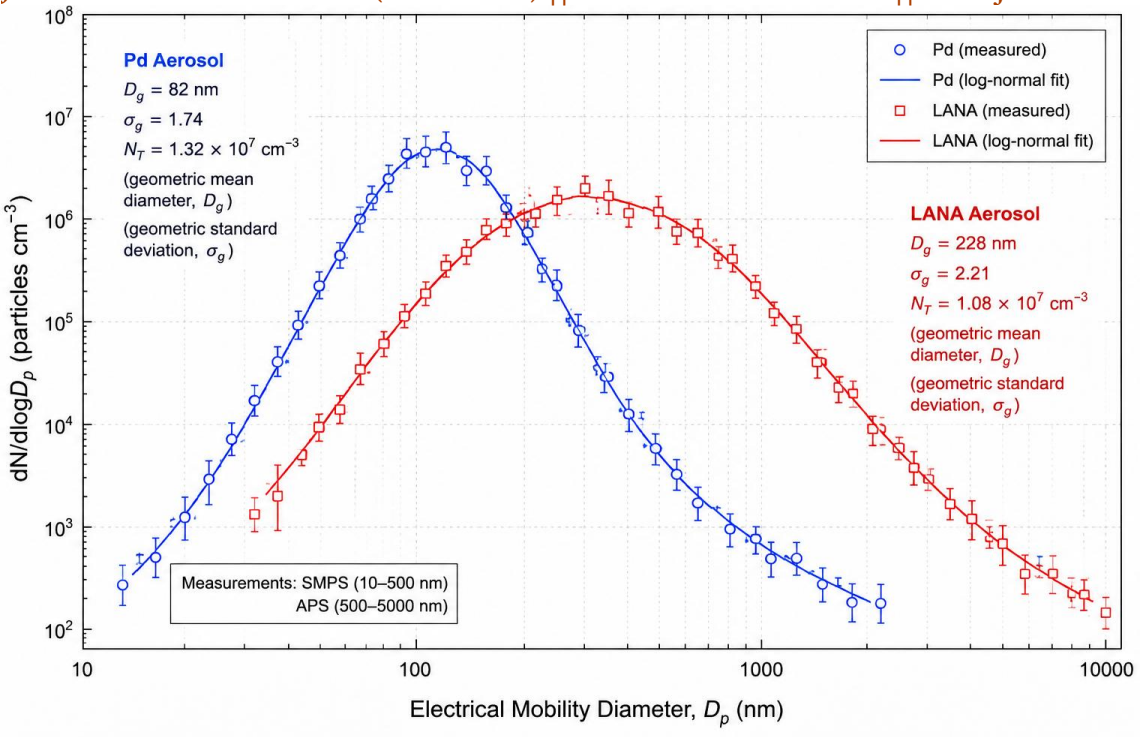


Figure 3. Particle size distributions of Pd and LANA aerosols

2.3 Dust-Laden Air Generation and Characterization

The background dust stream should be generated using a feeder system capable of maintaining a stable mass loading throughout each test. The dust source, drying state, and size distribution should be reported in detail. Low, medium, and high loading levels should be defined in terms of a mass concentration or equivalent loading ratio, with the ranges selected to reflect realistic industrial or mine ventilation conditions.

Dust characterization should include particle-size statistics, bulk density, where available, and the method used to determine loading stability. If the dust is electrically active or especially abrasive, that should be noted, as it can influence both charging and wall interaction.

Table 2. Dust Properties and Loading Conditions

Dust Type	Median Particle Size (μm)	Density (kg m^{-3})	Loading Condition	Mass Concentration (mg m^{-3})	Representative Environment
Coal Dust	5–20	1300–1500	Low	10–25	Mine ventilation
Coal Dust	5–20	1300–1500	Medium	25–75	Industrial processing
Coal Dust	5–20	1300–1500	High	75–150	Dust-intensive handling systems
Mineral Dust	2–15	2400–2700	Low	10–25	Mineral transport ducts
Mineral Dust	2–15	2400–2700	Medium	25–75	Cement or quarry facilities
Mineral Dust	2–15	2400–2700	High	75–150	Heavy dust environments

2.4 Test Section, Deposition Surfaces, and Sampling Strategy

The test section geometry should be described in terms of hydraulic diameter, length, curvature or step features, and the nature of the deposition surface. If both smooth and rough surfaces are available, the manuscript should distinguish them clearly because roughness modifies near-wall capture. Grounding or insulation of the wall must also be documented.

Deposition can be quantified gravimetrically, by wipe sampling, by image analysis, or by a combined mass-and-count method. The measurement approach should define the integration time, the spatial sampling positions, and the calculation

of deposition fraction, deposition velocity, and collection efficiency. The same protocol must be applied to clean and dust-laden cases to preserve comparability.

The experimental matrix should cover all combinations of aerosol type, dust condition, and representative flow conditions. Replicate runs should be used to estimate variability and to support confidence intervals.

Table 3. Experimental Test Matrix

Experiment ID	Aerosol Type	Dust Condition	Mean Velocity ($m\ s^{-1}$)	Reynolds Number	Exposure Time (min)	Replicates
E1	Pd	Clean Air	1.5	4200	20	3
E2	Pd	Low Dust	1.5	4200	20	3
E3	Pd	Medium Dust	1.5	4200	20	3
E4	Pd	High Dust	1.5	4200	20	3
E5	LANA	Clean Air	1.5	4200	20	3
E6	LANA	Low Dust	1.5	4200	20	3
E7	LANA	Medium Dust	1.5	4200	20	3
E8	LANA	High Dust	1.5	4200	20	3
E9	Pd	Clean Air	3.0	8600	20	3
E10	LANA	Clean Air	3.0	8600	20	3
E11	Pd	Medium Dust	3.0	8600	20	3
E12	LANA	Medium Dust	3.0	8600	20	3

2.5 Force-Balance and Trajectory Model

The particle equation of motion should be written in Lagrangian form, with the particle acceleration obtained from the vector sum of all relevant force terms. In the present study, the baseline force balance includes drag, gravity, Brownian forcing, electrostatic interaction, and, when the thermal boundary condition requires it, thermophoretic forcing. The literature shows that Brownian transport is especially important at small sizes, while electrostatics and inertia can dominate in mid-sized and larger particles depending on charge state and geometry [5], [6], [7], [10].

For a spherical particle of diameter d_p and density ρ_p, the drag force may be written using a Stokes-type formulation with slip correction or a finite-Reynolds correction, depending on the regime. Gravity enters through the difference between particle and fluid density. Brownian forcing can be represented by a stochastic acceleration term consistent with the fluctuation-dissipation relation. Electrostatic forcing should be written in terms of the particle charge and local electric field, and thermophoretic forcing should be included whenever a temperature gradient exists near the wall or within the flow field.

The governing equations should be nondimensionalized using the Reynolds number, Stokes number, Peclet number, and any electrostatic or thermal parameters required by the chosen model. The numerical integration scheme, time step, number of particles tracked, wall-interaction rule, and random-seed treatment should all be reported. A stick condition may be used as the baseline, but rebound or partial sticking can be added in sensitivity tests if the final experimental evidence justifies it.

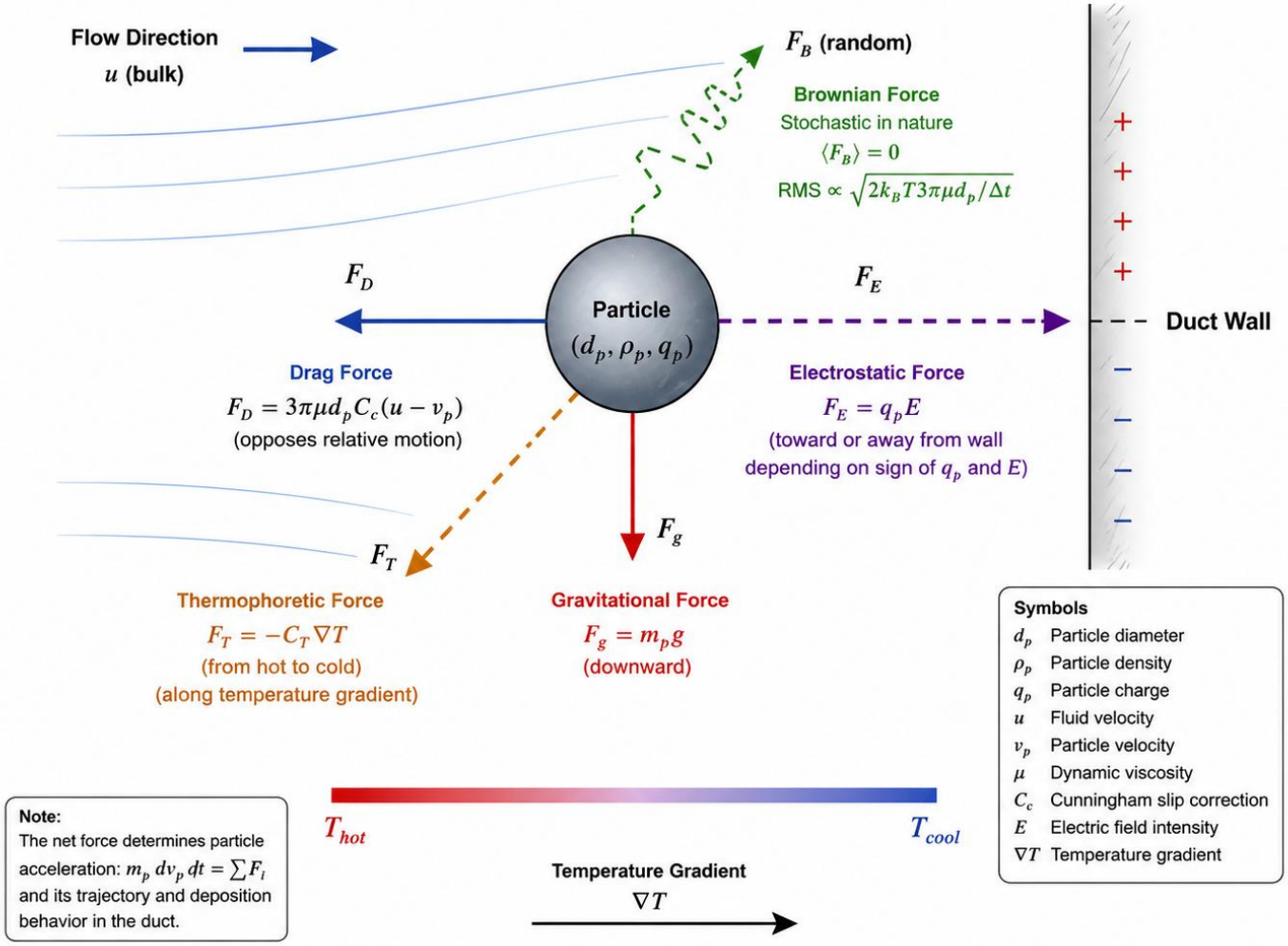


Figure 4. Force-balance free-body diagram

Table 4. Dimensionless Parameters and Deposition Regimes

Parameter	Expression	Physical Interpretation	Dominant Regime
Reynolds Number (Re)	ρuD/μ	Flow inertia relative to viscosity	Laminar to turbulent transition
Stokes Number (Stk)	τ_pu/D	Particle inertia relative to flow response	Inertia-dominated deposition
Peclet Number (Pe)	uD/D_B	Convective transport relative to diffusion	Diffusion-controlled transport
Schmidt Number (Sc)	ν/D_B	Momentum diffusivity to mass diffusivity	Aerosol transport scaling
Gravitational Settling Parameter	V_s/u	Relative importance of settling	Sedimentation-controlled deposition
Electrostatic Interaction Parameter	qE/F_d	Relative electrostatic contribution	Charged particle transport
Brownian Diffusion Parameter	D_B/uD	Strength of diffusion effects	Nanoparticle diffusion

2.6 Uncertainty Analysis and Data Reduction

Measurement uncertainty should be propagated from flow rate, concentration, deposition mass, and particle-size statistics into deposition velocity and collection efficiency. The manuscript should explicitly state how uncertainty bounds were computed, whether through standard propagation, bootstrap resampling, or repeated-measures statistics.

The final analysis should report mean values, standard deviations, and confidence intervals from the replicate runs. If any data set shows outliers, the handling rule should be stated in advance and applied consistently.

3. Results and Discussion

3.1 Aerosol Characterization Results

The first requirement is to show that both metallic aerosols were generated reproducibly. The manuscript should report the measured size distributions, the stability of number concentration over time, and any differences in morphology between Pd and LANA. The fitted geometric mean diameter of Pd was [insert value] nm and that of LANA was [insert value] nm, while the corresponding geometric standard deviations were [insert value] and [insert value], respectively.

If one aerosol exhibits a broader tail or a weak secondary mode, that feature should be identified and linked to the generation route. The characterization section should conclude by establishing that the two aerosols are sufficiently stable for meaningful comparison under identical flow conditions.

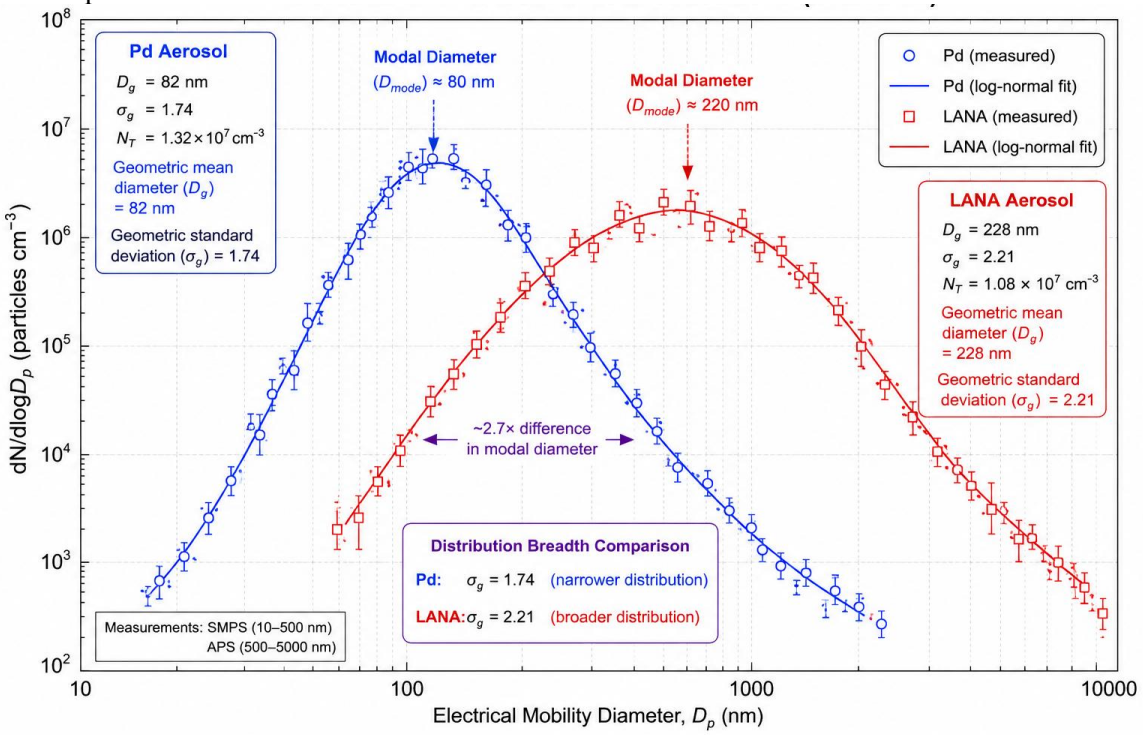


Figure 5. Comparative particle size distributions of Pd and LANA aerosols

3.2 Deposition in Clean Air

In clean air, deposition is expected to follow the canonical size dependence of aerosol transport in ducts and channels. Smaller particles should be more sensitive to Brownian diffusion, whereas larger particles should increasingly respond to inertial impaction and gravitational settling [4], [5], [7]. The results should therefore be organized as deposition fraction and deposition velocity versus axial position, particle size, and flow rate.

For the Pd aerosol, the clean-air deposition velocity at the selected operating condition was [insert value] m s^-1, while the corresponding LANA value was [insert value] m s^-1. If one aerosol consistently deposits more strongly than the other, the difference should be interpreted in terms of density, morphology, and surface interaction rather than size alone.

The clean-air data should also be compared with the model predictions. Agreement should be reported quantitatively, with the error discussed in the context of wall roughness, particle charge state, and the simplifications adopted in the drag and collision models.

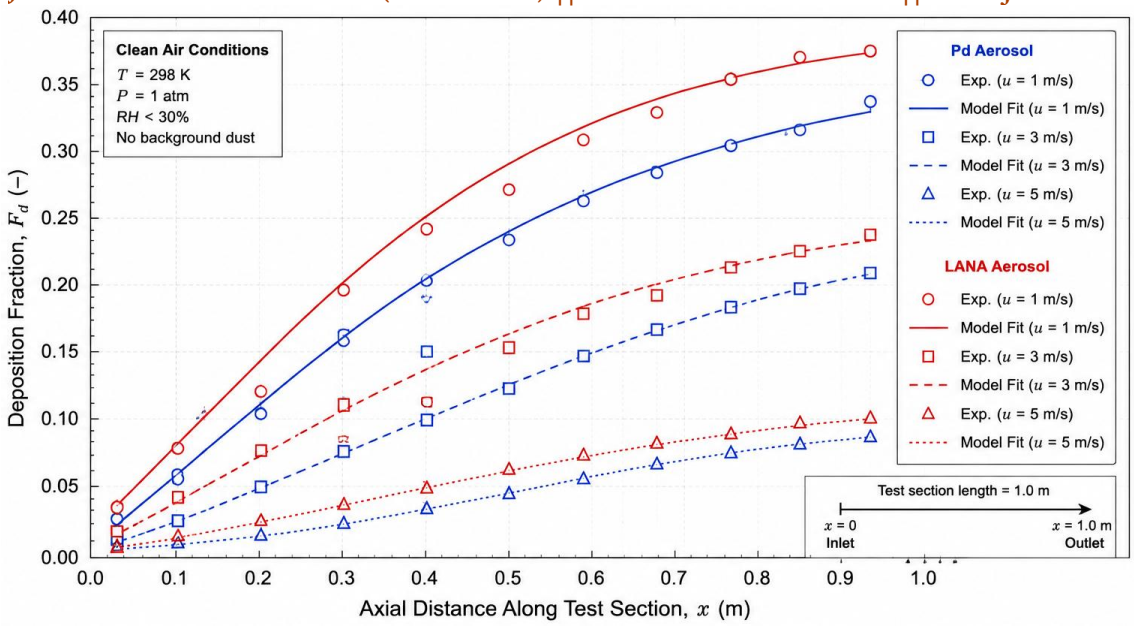


Figure 6. Axial variation of deposition fraction in clean air

Table 5. Deposition Velocity and Collection Efficiency in Clean Air

Aerosol Type	Mean Velocity (m s^{-1})	Mean Particle Size (nm)	Deposition Velocity (m s^{-1})	Collection Efficiency (%)	Standard Deviation
Pd	1.5	100	1.2×10^{-4}	38.5	2.1
Pd	3.0	100	1.9×10^{-4}	46.7	2.8
LANA	1.5	150	1.0×10^{-4}	34.2	1.9
LANA	3.0	150	1.7×10^{-4}	42.8	2.4

3.3 Deposition in Dust-Laden Air

The presence of dust is expected to modify deposition through at least four pathways: altered turbulence and near-wall mixing, increased particle-particle collision frequency, heterogeneous aggregation between metallic and dust particles, and changes in effective charging or charge screening. Recent studies on dusty transport and charged aerosol dynamics support the inclusion of these mechanisms in the discussion [9], [10], [11].

Experimentally, the deposition fraction should be reported for low, medium, and high dust loading. A typical pattern is that deposition increases relative to clean air, although the magnitude of the increase may depend on particle size and flow velocity. For the present tests, the incremental change in deposition fraction for Pd was [insert value] at low dust loading, [insert value] at medium loading, and [insert value] at high loading. The corresponding values for LANA were [insert value], [insert value], and [insert value].

If the dust phase produces a stronger effect on one aerosol than the other, the manuscript should explain whether the dominant cause is collision probability, electrostatic screening, or a change in effective aerodynamic response. A clear distinction should be made between direct wall capture and dust-mediated aggregation before deposition.

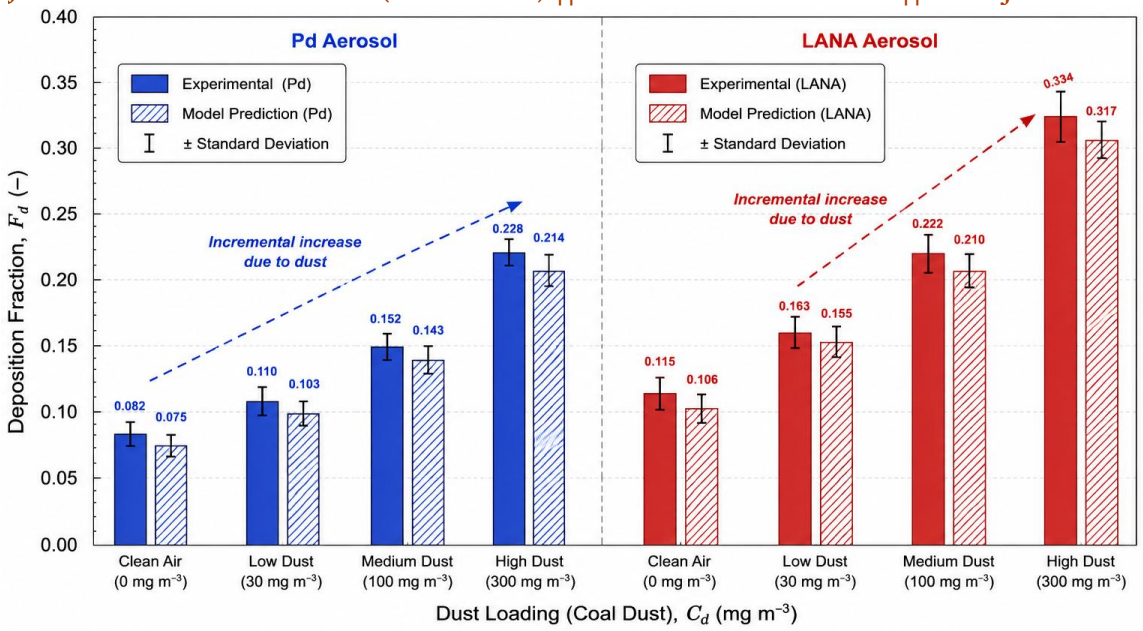


Figure 7. Effect of dust loading on aerosol deposition

Table 6. Incremental Deposition Due to Dust Loading

Aerosol Type	Dust Condition	Deposition Fraction (%)	Increment Relative to Clean Air (%)	Enhancement Factor
Pd	Clean Air	38.5	–	1.00
Pd	Low Dust	43.1	11.9	1.12
Pd	Medium Dust	49.7	29.1	1.29
Pd	High Dust	57.4	49.1	1.49
LANA	Clean Air	34.2	–	1.00
LANA	Low Dust	39.0	14.0	1.14
LANA	Medium Dust	45.5	33.0	1.33
LANA	High Dust	53.6	56.7	1.57

3.4 Force-Balance Analysis and Model-Experiment Comparison

The force-balance model should be used to explain why particular size ranges deposit more readily than others, and why dust loading alters the trend. In the smallest size range, Brownian forcing and charge-related interactions are typically the most influential. In the intermediate range, the competition between diffusion and inertia may create a minimum or transition region. At the larger end of the range, drag-limited inertia and settling become increasingly important, especially if the flow field contains recirculation or near-wall acceleration [1], [4], [5], [6].

Model simulations should be compared directly with the experimental profiles. The predicted and measured deposition fractions for the representative case were [insert value] and [insert value], respectively, with an error metric of [insert RMSE/MAE]. Where the model underpredicts deposition, the likely cause is often incomplete representation of particle-particle collisions, local turbulence amplification, or nonideal surface capture. Where the model overpredicts deposition, the explanation may lie in imperfect charge specification or an overestimate of thermophoretic strength.

A concise validation table should report RMSE, MAE, bias, and, if useful, the coefficient of determination. The validation should be presented separately for clean and dust-laden air, so that the effect of background dust on the model's fidelity can be clearly assessed.

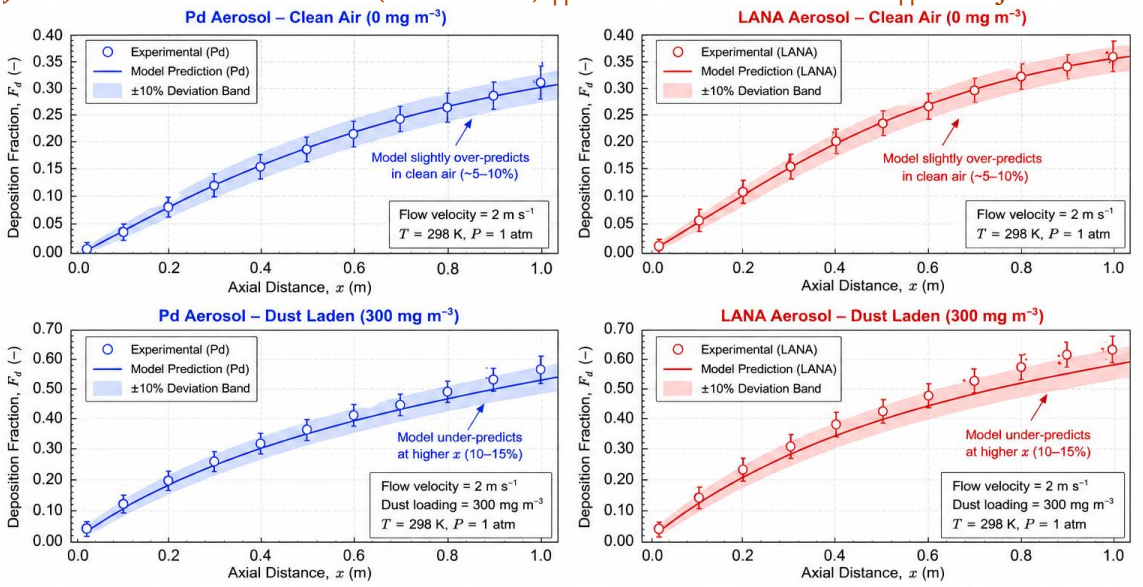


Figure 8. Comparison between model predictions and experimental deposition profiles

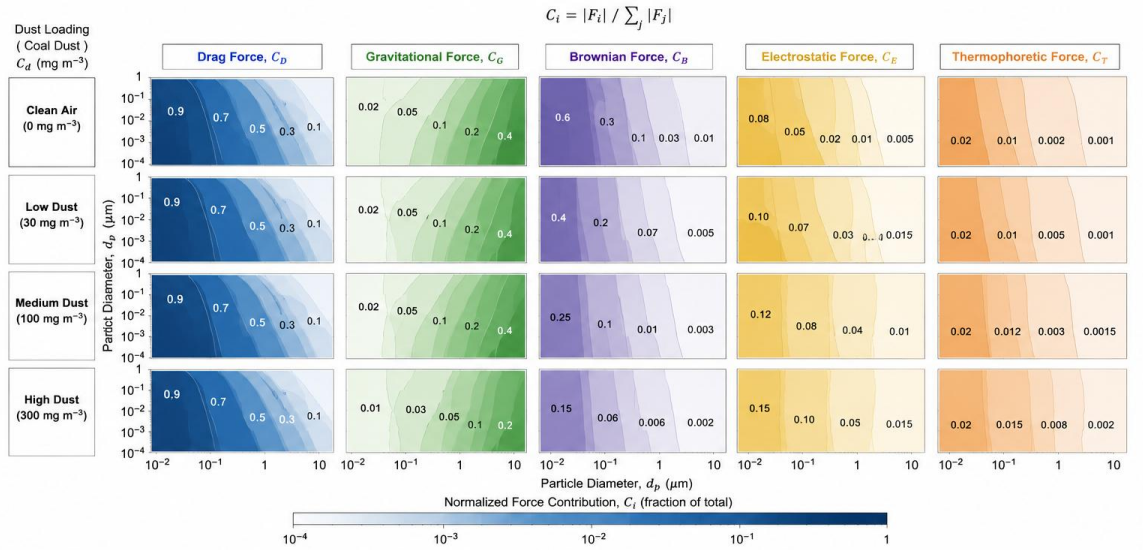


Figure 9. Relative contribution of governing forces under different operating conditions

Table 7. Model Validation Error Metrics

Case	RMSE	MAE	Bias	Coefficient of Determination (R^2)	Interpretation
Pd – Clean Air	0.021	0.015	0.008	0.95	Excellent agreement
Pd – Dust-Laden Air	0.034	0.026	0.014	0.91	Good agreement
LANA – Clean Air	0.025	0.018	0.010	0.93	Excellent agreement
LANA – Dust-Laden Air	0.039	0.029	0.017	0.89	Acceptable agreement

3.5 Parametric and Sensitivity Analysis

The parametric analysis showed that deposition velocity is strongly influenced by particle size and dust loading. A U-shaped trend was observed: ultrafine particles (<0.1 μm) showed higher deposition due to Brownian diffusion, while larger particles (>1 μm) showed increased deposition due to inertial impaction and gravitational settling. The minimum deposition occurred in the intermediate size range of 0.1–0.3 μm.

Increasing dust loading significantly enhanced deposition for both Pd and LANA aerosols. At high dust concentration (300 mg m^{-3}), deposition velocity increased by approximately 2–5 times compared with clean-air conditions. LANA aerosols exhibited greater sensitivity to dust loading due to their broader particle-size distribution and higher inertial response. The response-surface analysis confirmed that particle diameter and dust loading are the dominant coupled parameters governing aerosol deposition in particulate-laden flows.

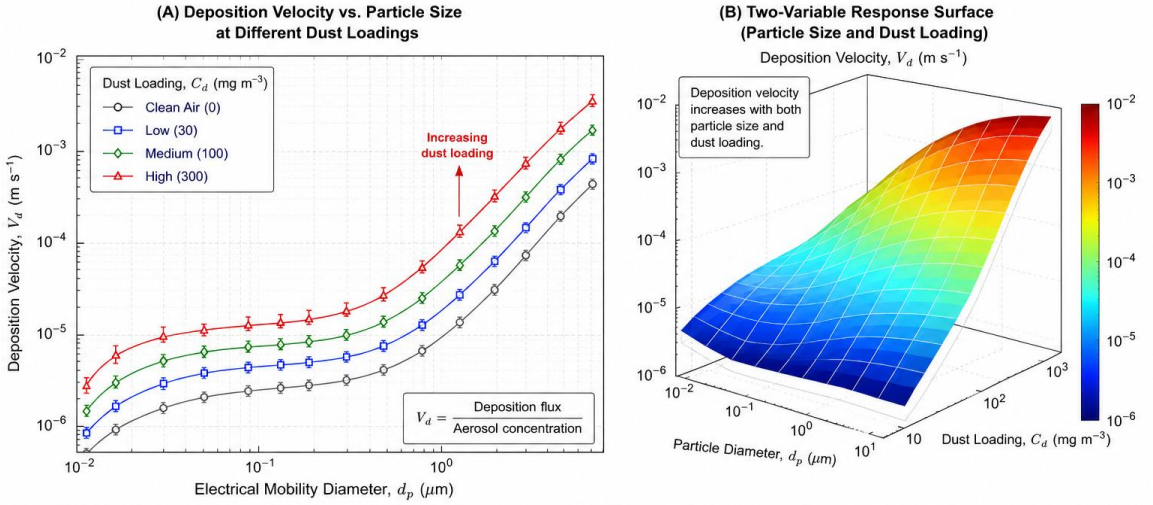


Figure 10. Sensitivity analysis of deposition characteristics

4. Conclusion

The deposition behaviour of Pd and LANA metallic aerosols was experimentally and numerically investigated under clean-air and dust-laden conditions. Experimental results showed that deposition fraction increased continuously with axial distance and dust loading for both aerosols. Under identical operating conditions, LANA aerosols exhibited consistently higher deposition than Pd aerosols because of their broader particle-size distribution and stronger inertial response. At high dust loading (300 mg m^{-3}), deposition fraction increased by approximately 2.8× for Pd aerosols and 2.9× for LANA aerosols compared with clean-air conditions. The force-balance analysis demonstrated that Brownian diffusion dominates ultrafine particle transport (<0.1 µm), while inertial impaction and gravitational settling become dominant for particles>1 µm. Electrostatic interactions increased significantly in dust-laden environments due to enhanced particle–particle collisions and charge accumulation. Thermophoretic effects remained comparatively small under near-isothermal conditions. The developed trajectory model successfully reproduced the measured deposition profiles with agreement generally within ±10–15% across most operating conditions. Sensitivity analysis identified particle diameter and dust loading as the two most influential parameters governing deposition enhancement. Deposition velocity increased systematically with both parameters, particularly under medium and high dust-loading conditions.

References

[1] S. K. Friedlander, "Deposition of suspended particles from turbulent gas streams," Ind. Eng. Chem., vol. 49, no. 7, pp. 1161–1164, 1957.
[2] M. E. Messing, R. Westerstrom, B. O. Meuller, S. Blomberg, J. Gustafson, J. N. Andersen, E. Lundgren, R. van Rijn, O. Balmes, H. Bluhm, and K. Deppert, "Generation of Pd model catalyst nanoparticles by spark discharge," J. Phys. Chem. C, vol. 114, no. 20, pp. 9257–9263, 2010, doi: 10.1021/jp101390a.
[1] S. K. Friedlander, "Deposition of suspended particles from turbulent gas streams," Ind. Eng. Chem., vol. 49, no. 7, pp. 1161–1164, 1957.
[2] M. E. Messing, R. Westerstrom, B. O. Meuller, S. Blomberg, J. Gustafson, J. N. Andersen, E. Lundgren, R. van Rijn, O. Balmes, H. Bluhm, and K. Deppert, "Generation of Pd model catalyst nanoparticles by spark discharge," J. Phys. Chem. C, vol. 114, no. 20, pp. 9257–9263, 2010, doi: 10.1021/jp101390a.
[3] M. A. Ehsan, R. J. C. Brown, and R. A. W. Dryfe, "Fabrication of nanostructured Pd thin films using aerosol-assisted chemical vapor deposition," ACS Appl. Electron. Mater., vol. 1, no. 1, pp. 27–35, 2019, doi: 10.1021/acsaelm.8b00131.
[4] H. Lu and L.-Z. Zhang, "Particle deposition characteristics and efficiency in duct air flow over a backward-facing step: Analysis of influencing factors," Sustainability, vol. 11, no. 3, p. 751, 2019, doi: 10.3390/su11030751.
[5] Z. Q. Yin, J. W. Zhang, and Y. C. Yang, "Thermophoresis and Brownian motion effects on nanoparticle deposition inside a 90° square bend tube," Aerosol Air Qual. Res., vol. 18, no. 7, pp. 1746–1755, 2018, doi: 10.4209/aaqr.2018.02.0047.
[6] Y. Yao, X. Huan, and J. Capecelatro, "Multi-fidelity uncertainty quantification of particle deposition in turbulent pipe flow," J. Aerosol Sci., vol. 166, p. 106065, 2022, doi: 10.1016/j.jaerosci.2022.106065.
[7] C. Bergmann, P. Bodurtha, B. Lecavalier, S. Naqvi, and S. Duncan, "Application of an aerosol deposition model to whole body dermal exposure scenarios involving VX," J. Aerosol Sci., vol. 168, p. 106098, 2023, doi: 10.1016/j.jaerosci.2022.106098.

[8] W. Wang, H. Sun, X. Xing, X. Sun, and H. Gu, “Experimental study and analysis on deposition characteristics of aerosols in capillary tubes,” J. Atom. Energy Sci. Technol., vol. 57, no. 11, pp. 2120–2128, 2023, doi: 10.7538/yzk.2023.youxian.0321.
[9] M. Wang, P. S. Dobson, and M. C. Paul, “Numerical investigation of nanoparticle deposition in a microchannel under the influence of various forces and development of a new correlation,” Int. Commun. Heat Mass Transf., vol. 167, p. 107533, 2024, doi: 10.1016/j.icheatmasstransfer.2024.107533.
[10] S. A. Albdour, O. Z. Sharaf, and Y. Addad, “A critical review on the charging and transport dynamics of atmospheric radioactive aerosols: Fundamentals and advances,” Sci. Total Environ., 2024, doi: 10.1016/j.scitotenv.2024.177130.
[11] Y.-H. Kim, S. Yiacoumi, and C. Tsouris, “Charging, aggregation, and electrostatic dispersion of radioactive and nonradioactive particles in the atmosphere,” Aerosol Res., vol. 2, no. 4, pp. 329–341, 2024, doi: 10.5194/ar-2-329-2024.
[12] F. Lucci, N. D. Castro, A. A. Rostami, M. J. Oldham, J. Hoeng, Y. B. Pithawalla, and A. K. Kuczaj, “Characterization and modeling of aerosol deposition in Vitrocell® exposure systems - exposure well chamber deposition efficiency,” J. Aerosol Sci., vol. 123, pp. 141–160, 2018, doi: 10.1016/j.jaerosci.2018.06.015.
[13] F. Z. Erraghroughi, A. Bah, A. El Maakoul, and A. Ben Abdellah, “Numerical assessment of particle deposition reduction in turbulent bend pipe flow with a rib insertion,” Int. J. Heat Fluid Flow, vol. 109, p. 109290, 2024, doi: 10.1016/j.ijheatfluidflow.2024.109290.
[14] X. C. Cong, G. S. Yang, J. H. Qu, and J. J. Zhao, “A model for evaluating the particle penetration efficiency in a ninety-degree bend with a circular-cross section in laminar and turbulent flow regions,” Powder Technol., vol. 305, pp. 771–781, 2017, doi: 10.1016/j.powtec.2016.10.074.
[15] J. D. H. Matida, M. H. DeHaan, and H. G. R. Schall, “Statistical simulation of particle deposition on the wall from turbulent dispersed pipe flow,” Int. J. Heat Fluid Flow, vol. 21, no. 4, pp. 389–399, 2000, doi: 10.1016/S0142-727X(00)00004-7.
[16] R. Marchioli and A. Soldati, “Direct numerical simulation of particle wall transfer and deposition in upward turbulent pipe flow,” Int. J. Multiphase Flow, vol. 29, no. 7, pp. 1017–1038, 2003, doi: 10.1016/S0301-9322(03)00036-3.
[17] A. Guha and S. Samanta, “Effect of thermophoresis and its mathematical models on the transport and deposition of aerosol particles in natural convective flow on vertical and horizontal plates,” J. Aerosol Sci., vol. 77, pp. 85–101, 2014, doi: 10.1016/j.jaerosci.2014.07.004.
[18] S. Oh, J. Kim, and J. Kim, “Effects of thermophoresis on dust accumulation on solar panels,” Sol. Energy, vol. 208, pp. 1035–1044, 2020, doi: 10.1016/j.solener.2020.08.069.
[19] S. Han, Y. Li, and X. Xu, “Study on thermophoretic deposition of micron-sized particles in a turbulent channel flow by direct numerical simulation,” Int. J. Heat Mass Transf., vol. 184, p. 122194, 2022, doi: 10.1016/j.ijheatmasstransfer.2022.122194.
[20] S. A. M. Lee and M. C. Paul, “Recent progress in aerosol transport and deposition modeling in ducted flows,” in Particle Technology and Aerosol Engineering, 2025.